HydroGEN Seedling: Novel Chalcopyrites for Advanced Photoelectrochemical Water Splitting

Nicolas Gaillard
University of Hawaii / Hawaii Natural Energy Institute
2440 Campus Road, Box 368
Honolulu, HI 96822
Phone: 808-956-2342
Email: ngaillar@hawaii.edu

DOE Manager: Katie Randolph
Phone: 720-356-1759
Email: Katie.Randolph@ee.doe.gov

Contract No: DE-EE0008085

Subcontractors:
- University of Nevada, Las Vegas, Las Vegas, NV
- Stanford University, Stanford, CA

HydroGEN Energy Materials Network nodes:
- Lawrence Livermore National Laboratory, Livermore, CA
- National Renewable Energy Laboratory, Golden, CO
- Lawrence Berkeley National Laboratory, Berkeley, CA

Project Start Date: October 1, 2017
Project End Date: September 30, 2020 (subject to annual Go/NoGo decision)

Overall Objectives

The overarching goal of this project is to create a chalcopyrite-based, semi-monolithic, tandem hybrid photoelectrode device prototype that can operate for at least 1,000 hours with solar-to-hydrogen STH efficiency >10%. This effort is supported by advanced characterization and theoretical modeling to accelerate the development of materials and interfaces. Specifically, our program aims to:

- Develop high-throughput synthesis techniques to create efficient copper chalcopyrite-based materials with ideal optoelectronic properties for photoelectrochemical (PEC) water splitting
- Identify appropriate surface treatments to prevent photocorrosion, improve surface energetics, and facilitate the hydrogen evolution reaction
- Create a new method to integrate temperature-incompatible materials into a semi-monolithic PEC device structure.

Fiscal Year (FY) 2019 Objectives

- Synthesize new wide-bandgap chalcopyrite made of Cu, In, Al, and Se using printable molecular inks.
- Identify mechanisms responsible for improved durability and energetics in surface-modified chalcopyrites.
- Further develop the concept of transparent/conductive binders to serve as a binding material in the semi-monolithic integration scheme.

Technical Barriers

This project addresses the following technical barriers from the Fuel Cell Technologies Office Multi-Year Research, Development, and Demonstration Plan[1]:

- Materials Efficiency (AE)
- Materials Durability (AF)
- Integrated device configuration (AG)
- Synthesis and Manufacturing (AJ).

Technical Targets

In Task 1, we further evaluated the effect of alkali doping on point defects in $CuGa_3Se_5$ and developed wide-bandgap $Cu(In,Al,B)Se_2$ and developed a baseline "printing" process. In Task 2, we integrated non-precious catalytic-protecting layers and Cd-free buffers to enhance chalcopyrites' durability and charge separation efficiency, respectively. Finally, in Task 3, we tested the transparent conductive epoxy/particle composites developed in FY 2018 for semi-monolithic PEC device integration. The status of this project's technical targets is documented in Table 1.

[1] https://www.energy.gov/eere/fuelcells/downloads/fuel-cell-technologies-office-multi-year-research-development-and-22

FY 2019 Accomplishments

- Modeled various chemical defects in chalcopyrites and assessed their impact on optical and electrical properties.
- Evaluated Si doping on the efficiency and durability of $CuGa_3Se_5$ photocathodes.
- Analyzed printed chalcopyrites via advanced spectroscopy techniques, showing a reduction in surface contamination after post-annealing in selenium atmosphere.
- Performed continuous operation of a WO_3-coated $CuGa_3Se_5$ photocathode for over 6 weeks.
- Successfully fabricated highly conductive and transparent binders made of epoxy and silver particles.

INTRODUCTION

Our multidisciplinary program combines advanced synthesis techniques, unique characterization, and theoretical approaches to improve the efficiency and durability of chalcopyrite-based hybrid photoelectrode devices, with the final goal of producing a chalcopyrite-based, semi-monolithic device with at least 10% STH efficiency.

APPROACH

We aim to advance the performance of previously identified wide-bandgap chalcopyrite materials through alkali doping, as well as develop and test the water-splitting viability of the next generation of chalcopyrites. We also see the unrealized potential to improve the PEC/electrolyte interface energetics and stability, which is addressed by investigating alternative buffer materials and protective layers. Finally, to avoid the heat-stress issues facing all-chalcopyrite monolithic tandem devices, we investigate a semi-monolithic structure, which will utilize a transparent conductive bonding polymer and exfoliation technique to avoid exposing the bottom photovoltaic (PV) driver in these devices to the high temperatures required for wide-bandgap chalcopyrite synthesis.

RESULTS

Task 1: Modeling, Synthesis, and Characterization of Chalcopyrite Photocathodes

Modeling

The theoretical studies over the past year have aimed at improving the understanding of fundamental and defect-related properties of the absorbers and interfaces to correlate with the observed performance in the synthesized material and resulting devices. We have extensively considered the role of point defects in the parent chalcopyrite compounds of desirable top-cell absorber alloys (e.g., $Cu(In,Ga)S_2$) to investigate how synthesis conditions influence defect populations. This knowledge is critical to both targeting desired electrical properties and mitigating problematic traps and recombination centers; it also intimately depends on the chemical potentials of the atomic species during growth and post-processing steps. In Figure 1(a), we include the phase diagram of one parent compound, $CuGaS_2$, as calculated with advanced hybrid functionals and showing the phase boundaries with competing phases as a function of the Ga and Cu chemical potentials. We translate this information into the calculated formation energies of native defects in Figure 1(b), where we find significant regions in the phase diagram that yield a strong competition between Cu vacancies (V_{Cu}) acceptors, interstitial donors (Cu_i), and disorder where Cu incorporates as a deep acceptor antisite on the Ga sites (Cu_{Ga}). While high V_{Cu} concentrations are desirable for highly *p*-type absorbers, significant incorporation of defects exhibiting deep states within the bandgap like Cu_{Ga} may lead to unwanted sub-gap absorption, which is detrimental for absorbers in tandem devices. We continue to actively investigate the influence of the dominant defects (both intrinsic and extrinsic) on the optical and electrical properties as a function of growth and annealing conditions to identify mitigation strategies (e.g., passivation) or targeted synthesis conditions.

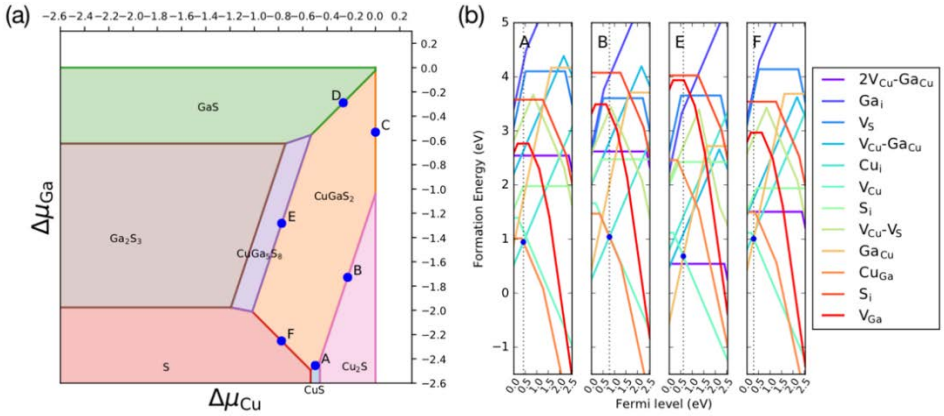

Figure 1. (a) Calculated phase diagram for $CuGaS_2$ as a function of Cu and Ga chemical potentials, showing the phase boundaries with competing phases. Formation energy diagrams of native defects shown as a function of the Fermi level are included in (b) corresponding to various points in the phase diagram. While more Cu-poor conditions favor the most p-type material (e.g. point F) owing to Cu vacancies (V_{Cu}), nominally more Cu-rich conditions can still yield considerable V_{Cu} and p-type conductivity, but also Cu_{Ga} antisites that exhibit localized states within the bandgap may detrimentally influence the optical transmission and impact performance in tandem cells.

Ordered vacancy compounds

The prospect of using Si doping to improve the PEC performance of $CuGa_3Se_5$ photocathodes was investigated. Evaporating Si onto the absorbers in situ led to the formation of $SiSe_2$, which immediately reacted to form SiO_2 and H_2Se when exposed to air ($SiSe_2 + 2\ H_2O \rightarrow SiO_2 + 2\ H_2Se$; as evidenced by the H_2Se gas that was detected when the co-evaporation chamber was vented). It is therefore likely that the $CuGa_3Se_5$ polycrystal surfaces are coated with thin SiO_2 layers, in agreement with a former report that found an accumulation of Si dopant at Cu(In,Ga)Se_2 grain boundaries. Chopped light linear sweep voltammetry (CLIV) characteristics of bare photocathodes (glass/Mo/$CuGa_3Se_5$) in 0.5 M H_2SO_4 under 1 Sun illumination (Figure 2) indicated that the addition of Si passivates the films. Si doping increased the onset potential by ~0.1 V and led to better photocurrents at 0 V vs. RHE, relative to the best baseline photocathode. It is unlikely that Si dopes grain interiors because the Si_{Cu} and Si_{Ga} substitution defects should donate electrons, whereas the absorbers were all p-type. Intrinsic $CuGa_3Se_5$ is p-type, and the Si-doped solar cells ($CuGa_3Se_5$/CdS p-n junctions) performed similarly to the baseline (not shown). The improvement in initial PEC performance is promising, as SiO_2 may also act as a protective layer that can improve the durability of the films due to its acid resistance. More characterization is underway to confirm the hypotheses that Si leads to electronic and chemical passivation.

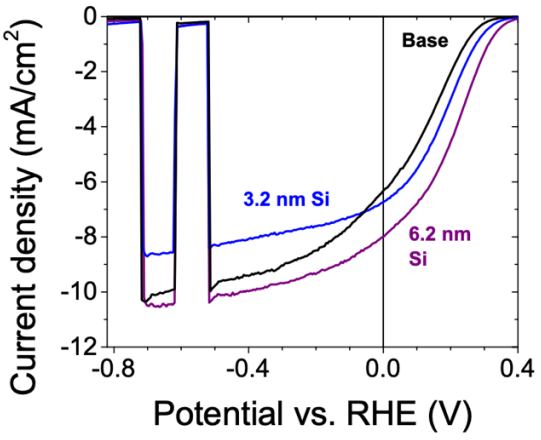

Figure 2. CLIV characteristics of standard photocathodes (glass/Mo/$CuGa_3Se_5$): the best baseline (black), 3.2 nm Si (blue) and 6.2 nm Si (purple).

Photophysical characterization

The optical properties of $CuInGaS_2$ thin film samples were investigated to determine their bandgap and sub-bandgap absorption (defect absorption). The ability to tune the optical bandgap of these materials enables optimization of the balance between light-harvesting efficiency and maximum photovoltage for driving hydrogen evolution from water splitting. We investigated the optical properties of the materials by photothermal deflection spectroscopy, a sensitive type of absorption spectroscopy (Figure 3). Here we observed a clear band onset at 1.91 eV with tailing from defect absorption. However, the maximum photovoltage can be limited by intrinsic defects in the material, which can vary for a given composition and growth/processing strategy. Therefore, a careful understanding of band position and related defects is critical to further the application of $CuInGaS_2$ materials for hydrogen production. To access intrinsic defects, we investigated the light emission properties of the films as a function of temperature down to 11 K. Typically, defect luminescence efficiency at room temperature is low yet at cryogenic temperature de-trapping by thermal excitation and non-radiative recombination can be minimized. From these measurements, two luminescence peaks were observed at 1.42 eV and 1.57 eV where can be related to deep trap states located at 340 meV and 490 meV below the band edges, respectively. Further work may seek to identify the origin of these defects, mitigation, and their relationship to function PEC performance.

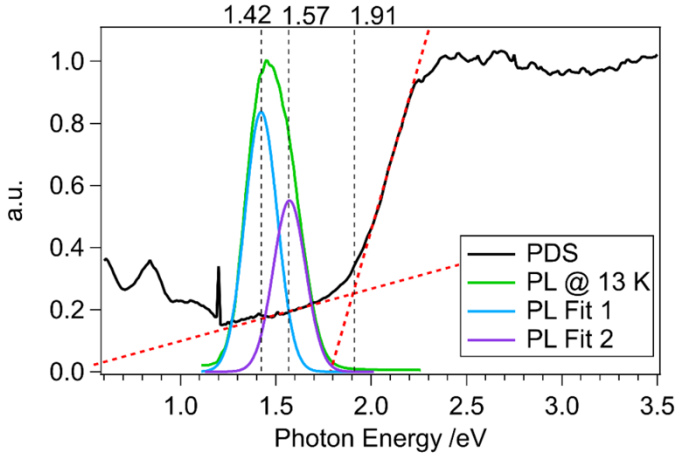

Figure 3. Photothermal deflection spectrum (black), taken at room temperature, and photoluminescence spectrum (green) of $CuInGaS_2$ on fluorinated tin oxide (FTO) glass, taken at 13 K. Also show are the two Gaussian peaks used to fit the PL spectrum centered at 1.42 and 1.57 eV.

Task 2: Interface Engineering for Enhanced Efficiency and Durability

X-ray photoelectron spectroscopy

In the second year of the project, University of Las Vegas (UNLV) continued to focus on characterizing HNEI-supplied samples using X-ray Photoelectron Spectroscopy (XPS, at UNLV) and X-ray Emission Spectroscopy (XES, at the Advanced Light Source, Lawrence Berkeley National Lab). Two sample sets, consisting of $CuInS_2$ and $CuIn(S,Se)_2$, were analyzed by the UNLV team. The $CuInS_2$ samples are precursors to the selenized $CuIn(S,Se)_2$ samples and are made by depositing a solution-based mixture, consisting of CuCl, $InCl_3$, and thiourea (CH_4N_2S), onto a molybdenum-coated soda-lime glass substrate. One sample set was synthesized in air and spin-coated in air (labeled as "Air"). A similar procedure was used to prepare the other sample set (labeled as "GB HPLC $CuInS_2$"); in contrast, however, the synthesis was done in a glove-box (GB), while the spin-coating was still performed in air. The "HPLC" abbreviation refers to the HPLC-grade methanol used to prepare these two samples. The XPS surveys of four samples from the two sets are shown in Figure 4 . For "Air" synthesis, the carbon signal is stronger; this is not unexpected, as the synthesis environment generally impacts the surface chemical environment found on exposed sample surfaces.

A similar trend can be seen at the near-surface bulk using XES (Figure 4). The oxygen and sodium signals in the XPS survey spectra also increase after selenization, and the Na signal is most pronounced for the sample

set synthesized in the glovebox. In contrast, the selenization process removes nitrogen and chlorine signals, likely due to the removal of excess starting materials. The reduction in nitrogen and chlorine after selenization can also be seen using XES (Figure 4), which gives insight into the chemical structure in the near-surface bulk. Furthermore, we find lateral inhomogeneities in the chemical composition (in particular the presence of Ca, Mo, and S signals) that can be correlated with the morphology of the different films under study. Figure 4 shows the XES spectra of three samples from the same two sample sets, each measured at two different spots. Using excitation energy of 380 eV, C K, Ca $L_{2,3}$, S $L_{2,3}$, Cl $L_{2,3}$, and Mo $M_{4,5}$ can be detected. Due to higher harmonics/orders from the undulator/beamline, N K emission can also be observed.

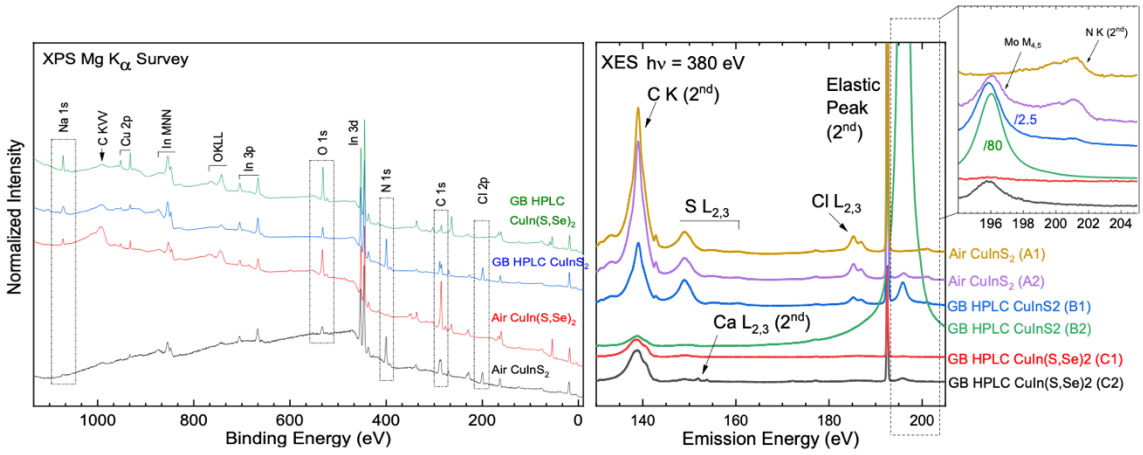

Figure 4. (left) XPS survey spectra of four samples: $CuIn(S,Se)_2$ and $CuInS_2$, with precursors synthesized in air ("Air") and in a glovebox ("GB HPLC"); both sample sets were then spin-coated in air, and Se-containing samples were further selenized. Prominent peaks are highlighted to emphasize changes between the different sample sets. (right) XES spectra of three samples, each measured at two different spots (A1, A2, etc.). C K, S $L_{2,3}$, Cl $L_{2,3}$, and Ca $L_{2,3}$ spectral features are labeled in the main graph. The exploded graph shows Mo $M_{4,5}$ and N K detail spectra (194–205 eV). For clarity, the intensity of the Mo $M_{4,5}$ peaks of the "GB HPLC CuInS2 (B2)" and "GB HPLC CuInS2 (B1)" was divided by 80 and 2.5, respectively. The label "2nd" indicates peaks observed in the second order of the spectrometer grating.

Development of tunable "buffers" via combinatorial methods

Due to the efforts in FY 2019, we now have a better understanding of the factors leading to the increased open-circuit voltage up to 925 mV for $Zn_{1-x}Mg_xO$-coated and Cd^{2+} surface-treated (Cd PE) $CuGa_3Se_5$ absorber devices. The effect of Cd PE on the $CuGa_3Se_5$ surface was investigated with XPS, UPS, and Kelvin probe at NREL. Ultraviolet to visible spectroscopy and Kelvin probe measurements were performed on $Zn_{1-x}Mg_xO$:Ga films to find the band positions. We found that NH_4OH treatment reduced surface oxidation. Cd PE treatment introduced Cd on the absorber surface. A reduction in Cu concentration suggested that Cd may be occupying Cu sites. Cd PE treatment moved the fermi level position upward in the absorber, indicating a change in surface conductivity type towards becoming intrinsic. The n-type counterpart for the p-type $CuGa_3Se_5$ absorber is possibly doped ZnO. Change of absorber surface conductivity type to either intrinsic or n-type may create a better p-i-n junction. The other notable outcome is the expected conduction band maxima upward shift in $Zn_{1-x}Mg_xO$ with increasing Mg composition. This reduces the conduction band offset between $CuGa_3Se_5$ absorber and $Zn_{1-x}Mg_xO$. We believe that, together, these two aforementioned beneficial factors are the reason for the improved V_{OC} of these devices.

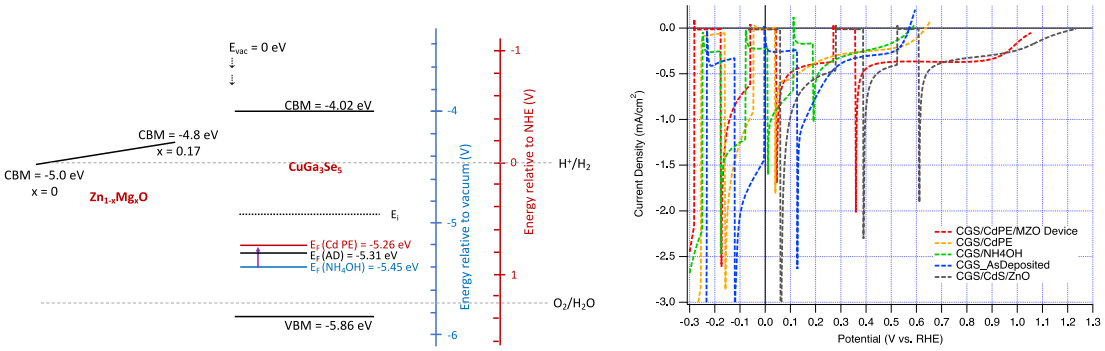

Figure 5. (left) CBM shift for $Zn_{1-x}Mg_xO$ with Mg composition, and energy band positions for $CuGa_3Se_5$ with different surface treatments. (right) three-electrode chopped light linear sweep voltammograms (LSV) measurement data for $CuGa_3Se_5/Zn_{1-x}Mg_xO$ devices.

Durability

During FY 2019, our team worked to develop protective coatings for PEC devices in acidic electrolyte conditions. This work focused on improving the durability of $CuGa_3Se_5$ photocathodes that were coated by atomic layer deposition with WO_3, which is predicted to have stability in acid. Figure 6 shows PEC measurements of two photocathodes: a bare $CuGa_3Se_5$ absorber and a $CuGa_3Se_5$ absorber that has been coated with an approximately 4 nm thick WO_3 layer and nanoparticulate Pt catalyst ($CuGa_3Se_5|WO_3|Pt$). The linear sweep voltammograms (LSV) in Figure 6a show that both electrodes demonstrate similar photocurrent onset at +0.3 V *vs*. RHE and reach a saturation photocurrent density (*j*) of about -8 mA/cm^2 under 1 Sun illumination. Figure 6b shows the constant illumination chronoamperometric (CA) durability testing of these same devices along with a replicate sample of each type, with the potential being held in the light-limited region for each. Both of the WO_3-coated CGSe devices achieved new durability records for any non-Si photocathode, bypassing 19,510°C cm^{-2} and 21,490°C cm^{-2} respectively over the course of the durability experiments, compared to 17,200°C cm^{-2} reported by our team on bare $CuGa_3Se_5$.[1]

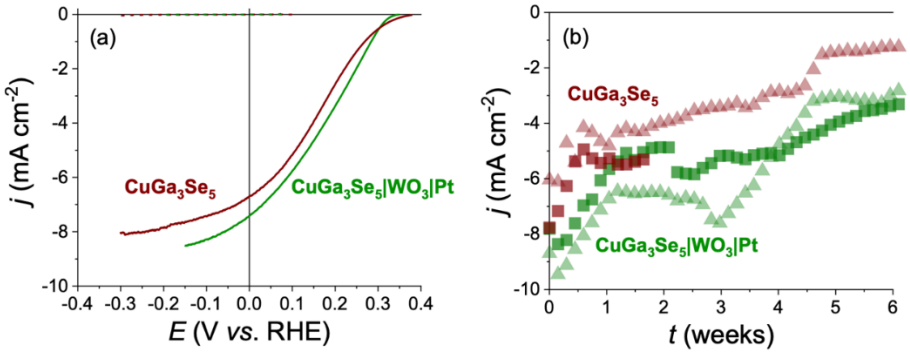

Figure 6. (a) LSV of a $CuGa_3Se_5/WO_3/Pt$ photocathode (green) and a bare $CuGa_3Se_5$photocathode (maroon) under hydrogen evolution reaction conditions, with their respective dark currents shown in dashed lines (overlapping the j=0 axis) (b) CA of these same devices held at constant potential, along with the CAs for a replicate sample of each type (light green and light maroon); all experiments were conducted under continuous 1 Sun illumination in 0.5 M sulfuric acid electrolyte with a $Hg/HgSO_4$ reference electrode and an Ir/IrO_x counter electrode, with hydrogen gas bubbling through the solution.

Task 3: Hybrid Photoelectrode Device Integration

The goal of this task is to solve process compatibility issues between material classes by bonding a chalcopyrite photoelectrode onto a fully processed PV driver. In the last fiscal year, we focused on the development of transparent conductive binders (TCBs) for semi-monolithic hybrid device integration. In this approach, the TCB is made by dispersing conductive media into a liquid epoxy. The TCB is then applied between the bottom and top cell, then cured to mechanically adhere to the two devices together, thereby

fabricating a semi-monolithic tandem device. During FY 2019, we explored a new approach to integrating the cells of a semi-monolithic device together. Where normally the liquid TCB would be cured after application, we have instead discovered a means to cure the liquid TCB prior to application to form a transparent conductive freestanding layer (TCFL), as shown in Figure 7. An advantage of using a TCFL as opposed to a TCB is that it eliminates potential spillover of the liquid TCB, which can lead to electrically shorting in the semi-monolithic device. The TCFL shown in Figure 7 was fabricated out of a TCB mixture of aluzine epoxy embedded with Ag-coated PMMA spheres. The amount of Ag-coated PMMA spheres present in the TCFL is such that the sum of the cross-sectional areas of the spheres equals 1% of the total cross-sectional area (referred to as 1% loading). Even with only 1% loading, these TCFLs exhibit excellent optical and electrical performance. Optically, the transmittance from 300–2,000 nm stays constant at approximately 90% for the entire range, considerably outperforming that of a standard commercially available fluorinated tin oxide (FTO) glass substrate, as seen in Figure 7. The TFCLs also exhibit excellent electrical conduction with an out-of-plane series resistance of 0.27 $\Omega.cm^2$, as seen in Figure 7.

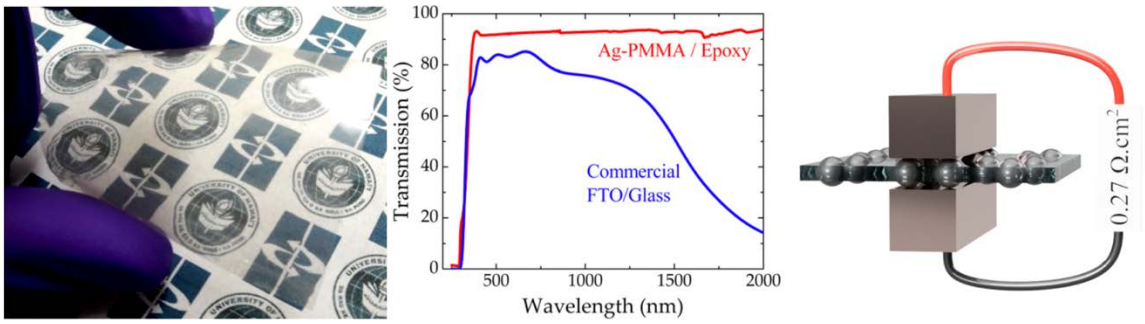

Figure 7. (Left) Image of a transparent conductive free-standing layer (Center) with high optical transmittance (T>90% in the 300–2,000 nm range) and (Right) out-of-plane series resistance (0.27 $\Omega.cm^2$) outperforming that of commercial FTO substrates.

CONCLUSIONS AND UPCOMING ACTIVITIES

- Further validate protection with WO_3 film, targeting 1,000 hrs of continuous operation.
- With help from advanced spectroscopy, improve our solution processing technique, aiming for high-efficiency wide-bandgap Cu(In,Al,B)Se_2 absorbers.
- Continue the development of ZnMgO buffers, targeting over 1V open-circuit voltage.
- Further develop the concept of semi-monolithic PEC device with improves transparent conductive binders.

FY 2019 PUBLICATIONS/PRESENTATIONS

1. N. Gaillard, "Emerging Chalcopyrite Photo-absorbers for Renewable Hydrogen Production," The 236th Electrochemical Society Meeting, Symposium I04, 1909, Atlanta (GA), 2019.
2. N. Gaillard, "Wide Bandgap Chalcopyrite-based Photoelectrodes for Renewable Hydrogen Production," The 2019 Spring Meeting of the European Materials Research Society (E-MRS), Symposium A "Latest Advances in Solar Fuels III", A.5.6, Nice (France), 2019.
3. N. Gaillard, "Wide Bandgap Chalcopyrites for Photoelectrochemical Water Splitting" The Materials Research Society Spring Meeting, Symposium ES11, ES11.05.03, Phoenix (AZ), 2019.
4. D. Palm, C. Muzzillo, N. Gaillard, T. Jaramillo, "Atomic Layer Deposited Tungsten-Based Coatings for Durable Solar Hydrogen Production," The 236th Electrochemical Society Meeting, Symposium I04, 1899, Atlanta (GA), 2019.

5. J. Varley, A. Sharan, T. Ogitsu, A. Janotti, A. Deangelis, N. Gaillard, “First-Principles Simulations of Stability, Optical and Electronic Properties of Competing Phases in Chalcopyrite-Based Photoelectrodes,” the 235th Electrochemical Society Meeting, Symposium I03, 1627, Dallas (TX), 2019.

REFERENCES

1. Muzzillo, C. P.; Klein, W. E.; Li, Z.; Deangelis, A. D.; Horsley, K.; Zhu, K.; Gaillard, N. "Low-Cost, Efficient, and Durable H2 Production by Photoelectrochemical Water Splitting with CuGa3Se5 Photocathodes," *ACS Appl. Mater. Interfaces*, *10* (23) (2018):19573–19579. https://doi.org/10.1021/acsami.8b01447.